Journal of Vertebrate Paleontology e2028796 (16 pages)

DOI: 10.1080/02724634.2021.2028796

ARTICLE

ALLOMETRIC ANALYSIS SHEDS LIGHT ON THE SYSTEMATICS AND ONTOGENY OF ANUROGNATHID PTEROSAURS

ZIXIAO YANG, [1,2] MICHAEL J. BENTON,[3] DAVID W. E. HONE,[4] XING XU,[5] MARIA E. McNAMARA,[2,6] and BAOYU JIANG[1,*]

[1]Center for Research and Education on Biological Evolution and Environments, School of Earth Sciences and Engineering, Nanjing University, Nanjing 210023, China, byjiang@nju.edu.cn;

[2]School of Biological, Earth and Environmental Sciences, University College Cork, Cork T23 TK30, Ireland, zyang@ucc.ie; maria.mcnamara@ucc.ie;

[3]School of Earth Sciences, University of Bristol, Life Sciences Building, Tyndall Avenue, Bristol BS8 1TQ, UK, mike.benton@bristol.ac.uk;

[4]School of Biological and Behavioural Sciences, Queen Mary University of London, Mile End Road, London E1 4NS, UK, d.hone@qmul.ac.uk;

[5]Key Laboratory of Vertebrate Evolution and Human Origins, Institute of Vertebrate Paleontology and Paleoanthropology, Chinese Academy of Sciences, Beijing 100044, China, xu.xing@ivpp.ac.cn;

[6]Environmental Research Institute, Lee Road, Cork T23 XE10, Ireland, maria.mcnamara@ucc.ie

ABSTRACT—Anurognathids are a clade of non-pterodactyloid pterosaurs with generally conservative morphology, but specializations as insectivores. They are represented by a disparate collection of adult and juvenile specimens that range in wingspan from ~0.24–1 m. There have been concerns about the extent to which ontogenetic variation might affect phylogenetic inference, and indeed how aspects of their ontogeny might relate to the distinctive anurognathid adult morphology. Here we perform allometric analysis on 23 key skeletal dimensions in 13 anurognathid specimens. Our results show that all anurognathids share a common growth trajectory in most dimensions, and that ontogeny affects variation in a minority of characters commonly used in phylogenetic analysis. Excluding these ontogeny-related characters, a new taxon, *Cascocauda rong* gen. et sp. nov., is established. Based on the ontogenetically corrected dataset, our phylogenetic analysis supports Anurognathidae as the sister-group of Breviquartossa and reveals a general trend of tail reduction in the clade. Allometric growth suggests the anurognathid lifestyle remained consistent throughout ontogeny, maintaining a highly maneuverable flight style by near-isometric development in the wing, small prey (i.e., insects), by strong negative allometry in the skull, and an arboreal habit by strong positive allometry in the claws. This specialized lifestyle suggests retention of plesiomorphic juvenile traits into later ontogeny and facilitated morphological stasis by stabilizing selection during over 40 million years of evolution in the group.

http://zoobank.org/urn:lsid:zoobank.org:pub:A65D6346ECFF-46C7-88F7-26AF99BBADD6

SUPPLEMENTAL DATA—Supplemental materials are available for this article for free at www.tandfonline.com/UJVP.

Citation for this article: Yang, Z., M. J. Benton, D. W. E. Hone, X. Xu, M. E. McNamara, and B. Jiang. 2022. Allometric analysis sheds light on the systematics and ontogeny of anurognathid pterosaurs. Journal of Vertebrate Paleontology. DOI: 10.1080/02724634.2021.2028796

INTRODUCTION

Anurognathids lived in Eurasian forests during the Middle Jurassic to Early Cretaceous (Hone, 2020). They shared a distinctive suite of morphological characters consistent with being specialized aerial insectivores active in low light conditions. These include (1) a wide mouth with a large gape and a sharp isodont dentition adapted for catching and holding insects (Bennett, 2007a; Ősi, 2011; Hone, 2020), (2) small size, a deep wing with curved wingtip and a short pliable tail, which together facilitated slow and highly maneuverable flight in dense forests (Bennett, 2007a; Ősi, 2011; Hone et al., 2015; Hone, 2020) and (3) large, anterolaterally directed eyes that were likely adapted for nocturnal and/or crepuscular predation (Bennett, 2007a; Lü et al., 2018). The gross morphology of anurognathids changed little during their 40-Ma existence, which suggested they had a rather conservative bauplan (Unwin et al., 2000; Bennett, 2007a; Hone, 2020).

Anurognathids are represented by 13 unequivocal specimens ranging from ~0.24–1 m in wingspan and of varying ontogenetic status. Nine specimens (including specimens of *Anurognathus*, *Dendrorhynchoides*, *Luopterus*, *Sinomacrops*, and *Batrachognathus*, and specimens NJU-57003 and CAGS-Z070 [Dalla Vechia, 2002; Yang et al., 2019; Hone, 2020; Wei et al., 2021]) show characteristics of immaturity, e.g., unfused articular bones, scapula-coracoid, pelvis and cranial elements. In contrast, the holotypes of *Jeholopterus* and *Vesperopterylus* show osteological maturity and are thus (sub)adults (Wang et al., 2002; Lü et al., 2018). Two specimens lack detailed descriptions, and their ontogenetic state is unknown (Gao et al., 2009; Jiang et al., 2015).

*Corresponding author.

Color versions of one or more of the figures in the article can be found online at www.tandfonline.com/ujvp.

Published online 03 Mar 2022

Inadequate recognition of ontogenetic status in previous studies of anurognathids has raised concerns about confounding ontogenetic variation with systematics (Hone, 2020). In particular, many length ratios used as diagnostic (e.g., Wang et al., 2002; Lü and Hone, 2012; Wei et al., 2021) or in analyzing characters (e.g., Kellner, 2003; Lü et al., 2018) may change greatly during growth (Delfino and Sánchez-Villagra, 2010). Previous statistical studies on ontogenetic changes in other pterosaurs have suggested or prompted taxonomic revisions for some taxa (e.g., Bennett, 1995, 1996, 2006, 2007b, 2013; Jouve, 2004; Vidovic and Martill, 2014). The prevalence of immature individuals in the known anurognathid dataset thus creates uncertainty regarding the validity of taxonomic assignments and may bias existing phylogenetic reconstructions.

Alternatively, if anurognathids share a common allometric growth pattern for particular elements, the known specimens would constitute a growth series from early juveniles to adults. This growth series would then provide a rare opportunity to explore ontogenetic development of morpho-function and understand the evolution of the distinctive anurognathid morphology. Indeed, studies on pterosaur allometry have already yielded insights into the relationship between skeletal proportions and biomechanics, particularly relating to aerodynamics, across taxa of different body sizes (e.g., Brower and Veinus, 1981; Padian and Warheit, 1989; Witton and Habib, 2010) and through growth of single species (e.g., Tomkins et al., 2010; Hone et al., 2020; Naish et al., 2021).

Here, we select skeletal dimensions used in previous diagnoses and phylogenetic analyses to test statistically whether anurognathid specimens share growth trajectories in various dimensions. By revealing which characters related to these dimensions are biased by ontogeny, a new specimen is assessed taxonomically excluding the biased characters. Critically, we compose a refined dataset for phylogenetic analysis by removing the recognized ontogenetic bias and updating with additional characters from recent studies. Our goals are to provide a more accurate understanding of anurognathid systematics and to explore how aspects of their ontogeny might affect the distinctive and conservative anurognathid adult morphology.

MATERIALS AND METHODS

Institutional Abbreviations—**BMNHC**, Beijing Museum of Natural History, Beijing, China; **BSP**, Bayerische Staatssammlung für Paläontologie und Geologie, Munich, Germany; **CAGS**, Chinese Academy of Geological Sciences, Beijing, China; **GMV**, National Geological Museum of China, Beijing, China; **IVPP**, Institute of Vertebrate Paleontology and Paleoanthropology, Beijing, China; **JPM**, Jinzhou Museum of Paleontology, Jinzhou, China; **JZMP**, Jinzhou Paleontological Museum, Jinzhou, China; **NJU**, Nanjing University, Nanjing, China; **PIN**, Palaeontological Institute, Russian Academy of Sciences, Moscow, Russia; **SMNS**, Staatliches Museum für Naturkunde Stuttgart, Stuttgart, Germany.

Anatomical Abbreviations—**aof**, antorbital fenestra; **cd**, caudal vertebrae; **ch**, chevron; **co**, coracoid; **cv**, cervical vertebrae; **dr**, dorsal rib; **dv**, dorsal vertebrae; **fe**, femur; **fi**, fibula; **fr**, frontal; **ga**, gastralia; **h**, humerus; **il**, ilium; **is**, ischium; **man**, mandible; **mci–iii**, metacarpal I–III; **mciv**, metacarpal IV; **mti–iv**, metatarsal I–IV; **mtv**, metatarsal V; **nar**, naris; **or**, orbit; **pa**, parietal; **pal**, palatine; **pdI–IV**, pedal digits I–IV; **pt**, pteroid; **ppu**, prepubis; **pu**, pubis; **pdV-1** and **2**, phalanges 1 and 2 of pedal digit V; **q**, quadrate; **r**, radius; **rp**, retroarticular process; **sc**, scapula; **scr**, sclerotic ring; **t**, tarsal; **th**, tooth; **ti**, tibia; **u**, ulna; **wp1–4**, wing phalanges 1–4; **z**, zygapophysis.

Measurements for Allometric Analysis

Twenty-three skeletal variables were measured from 13 anurognathid specimens (Fig. 1A and Supplemental Data 1): 1, skull length; 2, skull width; 3, scapula length; 4, coracoid length; 5, humerus length; 6, ulna or radius length; 7, pteroid length; 8, wing metacarpal length; 9, manual claw length; 10–13, length of first, second, third and fourth phalanx of wing finger, respectively; 14, femur length; 15, tibia length; 16, fibula length; 17, metatarsal length; 18, length of pedal digit III; 19, foot length = (metatarsal length + pedal digit III length); 20–21, length of first and second phalanx of pedal digit V, respectively; 22, length of pedal claw; 23, wingspan = (humerus + ulna/radius + metacarpal IV + wp1–4) × 2.1 (Lü et al., 2011).

Measurements were taken from the literature, photographs and, where possible, directly from specimens (see Supplemental Data 1 for details). Measurements from photographs were obtained using the image processing freeware ImageJ (available at http://rsbweb.nih.gov/ij/) and those from specimens were taken using a digital caliper; in both cases measurements were taken twice to ensure accuracy. Mean values were used for left and right elements when possible.

Tests for Allometric Correlation

All measurements were logarithmically transformed to evaluate the bivariate allometric relationship ($y = a \cdot x^b$) in the linearized form ($\log y = \log a + b \log x$). The standardized major axis (SMA) line-fitting method was applied to determine the allometric equation, and coefficients of determination (R^2) and probability values (p) were calculated to evaluate the strength and statistical significance of the correlation.

If the correlation was statistically significant ($p < 0.05$), we further tested the null hypothesis of isometry ($b = 1$). On account of the small sample size and unknown distribution of the allometric scaling coefficient (b), a bootstrap method (Plotnick, 1989) was applied with 1000 iterations to generate a one-tailed 95% confidence interval for b. We rejected the null hypothesis if the 95% confidence interval of b lay entirely above or below 1, i.e., positive or negative allometry, respectively. Otherwise, isometry was assumed. These were calculated in R v. 3.5.1 using the "smatr" (Warton et al., 2012), "dplyr" (Wickham et al., 2015), and "purrr" (Henry and Wickham, 2020) packages, using code given in the Supplemental Content.

As pterosaurs are forelimb-dominated launchers and fliers, humerus length has been used as a proxy for body mass and size (e.g., Wellnhofer, 1970, 1975; Wang et al., 2017). Here, humerus length was thus compared with most other variables in our pairwise bivariate analysis. Additional pairs yielding diagnostic length ratios in previous studies were also included (listed in Supplemental Data 2) and were tested, in the same way as those involving humerus length, for proportional change during growth in order to identify ontogenetic bias.

The data were further explored using principal components analysis (PCA) to assess whether humerus length is an appropriate body size proxy and the compatibility between allometric patterns resulting from bivariate and multivariate methods. Skeletal variables that did not return statistically significant allometric correlations in bivariate analysis were excluded from the PCA, since in these dimensions anurognathids show strong interspecific variation in growth trajectory. For the remaining skeletal variables, a covariance matrix of the log-transformed measurements was subjected to PCA to extract the first principal component (PC1) as an internally defined size variable; this accounted for every skeletal variable involved and allowed calculation of the allometric scaling coefficient for each skeletal variable (Jolicoeur, 1963; Klingenberg, 1996). Missing data were imputed using the iterative PCA method (Kiers, 1997), also

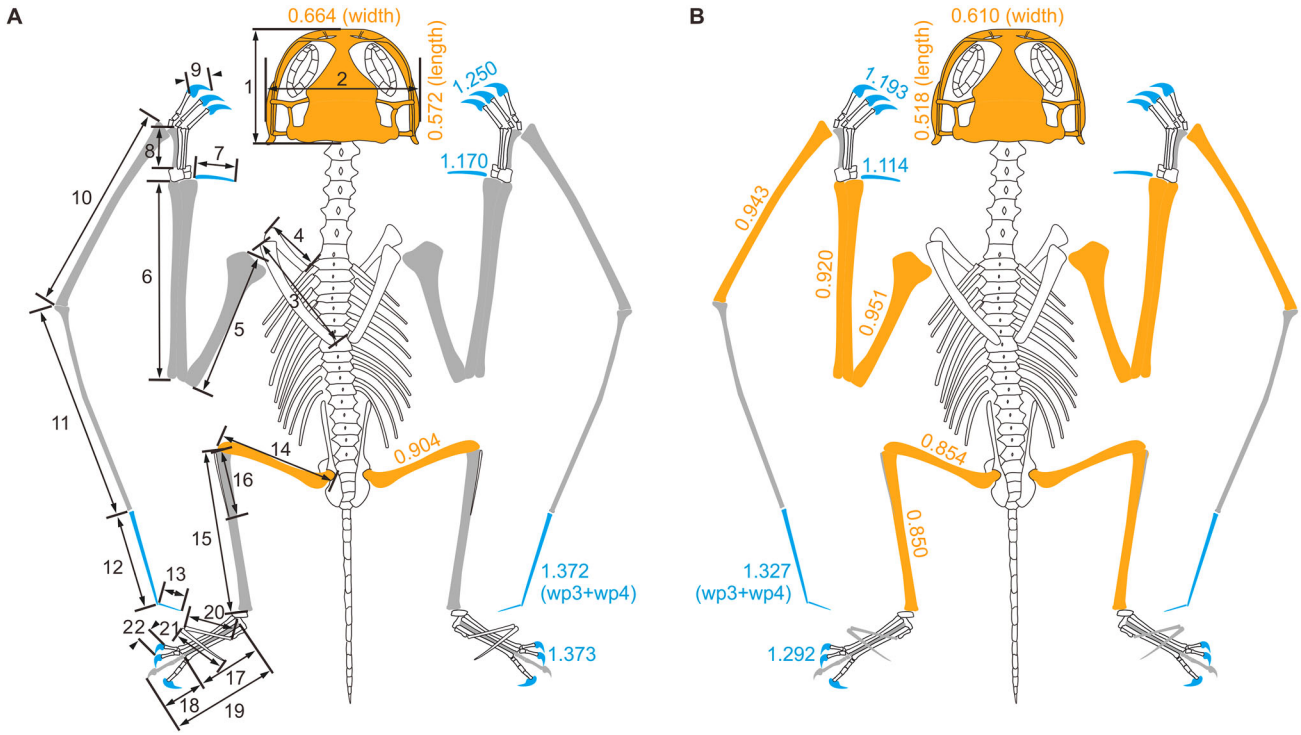

FIGURE 1. Allometric growth in anurognathids. **A**, line drawing of a generalized anurognathid showing measured skeletal dimensions and their allometric growth pattern relative to humerus; **B**, allometric growth pattern recovered by PCA. Allometric scaling coefficients are indicated next to the corresponding elements. Negative allometry, isometry, and positive allometry are indicated by orange, gray, and blue, respectively, in the online version of this article.

known as the EM-PCA algorithm (Josse and Husson, 2012); this is suitable for small datasets and provides better estimates than other imputation techniques when variables are highly correlated (Dray and Josse, 2015). The null hypothesis of isometry was then tested using the same scheme as in the bivariate analysis. The PCA was performed in R v. 3.5.1 using the "missMDA" (Josse and Husson, 2016) and "boot" (Canty and Ripley, 2021) packages, using code provided in the Supplemental Content.

Character Matrices

The data compiled for phylogenetic analysis were based largely on the character-taxon matrix from Longrich et al. (2018), which comprises 134 taxa and 271 characters and was copied and pasted into a Microsoft Excel file for editing. Considering that the present study focuses only on the phylogeny of Anurognathidae, we excluded non-pterodactyloid species with >50% missing data and pterodactyloid species with >25% missing data, leaving 36 species in the matrix. We added five anurognathids, *Luopterus mutoudengensis* (Lü and Hone, 2012; Hone, 2020), *Vesperopterylus lamadongensis* (Lü et al., 2018; Hone, 2020), *Sinomacrops bondei* (Wei et al., 2021), CAGS-Z070 (Ji and Yuan, 2002) and NJU-57003 (Yang et al., 2019), yielding a total of 41 taxa in the matrix.

Concerning the character (Char.) list, Char. 54 from Longrich et al. (2018) was deleted because the character description is likely incorrect: "Palate_anterior_end,_shape: absent present"; Char. 122 was deleted as it is a repetition of Char. 115. Further, we used the ratio of skull:humerus length for Char. 1 instead of skull:dorsal vertebra length as in the original dataset (Longrich et al., 2018). This is because (1) dorsal vertebrae are either missing or preserved with poorly defined boundaries in specimens of *Anurognathus*, *Luopterus*, *Sinomacrops*, *Dendrorhynchoides*, CAGS-Z070 and NJU-57003, (2) the skull:single vertebra length ratio is sensitive to measurement error, and (3) simply adding the skull:humerus length ratio to the character list would overweight the skull length in the analysis. The skull:humerus length ratio for non-anurognathid taxa was calculated by dividing the value for Char. 1 by that of Char. 28 in Longrich et al. (2018).

In order to incorporate as many characters as possible that were phylogenetically informative for anurognathid taxa, we evaluated each character in the original diagnosis and additional characters in Hone (2020) and Wei et al. (2021) (Supplemental Data 2) prior to inclusion in the character list (Supplemental Content). Characters were omitted if (1) they are uninformative (i.e., same states in all anurognathids), (2) the corresponding skeletal elements are poorly preserved, (3) they already exist in Longrich et al. (2018), or (4) they show allometric growth bias. The final character list (Supplemental Content) comprises 286 characters, including 17 newly added characters.

The original continuous characters (Longrich et al., 2018) were also checked for potential allometric growth bias, but the biased characters were not omitted from the character list because they are useful for determining phylogenetic relationships outside Anurognathidae. For each of the ontogeny-biased characters, we coded each anurognathid (with the corresponding anatomy preserved) with the same state as the largest specimen in order to remove the impact of such characters on taxonomy within Anurognathidae (Supplemental Data 3). An ontogenetically uncorrected matrix (i.e., using original states for each anurognathid) was compiled for comparison (Supplemental Data 4).

We recoded all four anurognathid taxa in the original dataset based on published specimen-specific descriptions and figures.

The coding of *Jeholopterus ningchengensis* was based on the holotype specimen IVPP V12705 (Wang et al., 2002) alone and the referred *Jeholopterus* specimen CAGS-Z070 (Ji and Yuan, 2002; Lü and Hone, 2012; Yang et al., 2019) was coded separately since its species assignment remains unclear. The coding of *Anurognathus ammoni* was based on the holotype BSP 1922 I 42 (Wellnhofer, 1975); a second specimen assigned to this species is from a private collection but has a cast specimen (SMNS 81928) available (Bennett, 2007a). The coding of *Batrachognathus volans* was based on the holotype PIN 52-2 (Bakhurina and Unwin, 1995; Unwin and Bakhurina, 2000) and a second specimen PIN 2585/4a (Costa et al., 2013) assigned to this species. The coding of *Dendrorhynchoides curvidentatus* was based on the holotype specimen of GMV 2128 (Ji and Ji, 1998). Codings of the recently named taxa, *Luopterus mutoudengensis*, *Vesperopterylus lamadongensis* and *Sinomacrops bondei* were based on their respective holotype specimens JZMP-04-07-3 (Lü and Hone, 2012), BMNHC-PH-001311 (Lü et al., 2018) and JPM-2012-001 (Wei et al., 2021), respectively.

Concerning the problematic tail in the holotype of *Dendrorhynchoides curvidentatus*, we agree with previous observations by Unwin et al. (2000) and Hone (2020) that only the proximal portion of the tail is genuine, where six disk-like vertebrae remain articulated and in contact with the sacrum, and that, based on the tapering of the proximal portion, the tail overall is short as in other short-tailed anurognathids and consists of fewer than 15 vertebrae. The distal portion of the tail, separated from the proximal portion by a gap, shows distinctly different morphology more typical of long-tailed pterosaurs and is considered artificial. Therefore codings for caudal morphology were based on the proximal portion (Chars. 24, 25, 208, 209, 210) and the tail:humerus length ratio was coded as unknown (Char. 49).

Concerning the controversial configuration of the external naris and antorbital fenestrae (i.e., separated vs. confluent) in anurognathids (e.g., Andres et al. 2010; Wei et al., 2021), this was coded as separated for NJU-57003 (based on present study) and *Anurognathus* (based on description by Bennett [2007a]), and as unknown for other anurognathids (Supplemental Data 3 and 4). For comparison, we composed a second matrix (Supplemental Data 5), based on the ontogenetically corrected data in Supplemental Data 3, in which NJU-57003 was coded as separated, *Batrachognathus volans*, *Sinomacrops bondei* and CAGS-Z070 as confluent (Wei et al., 2021), and as unknown for other anurognathids.

Phylogenetic matrices (Supplemental Data 3–5) in TNT format can also be found on the Morphobank page of this study (project 4151).

Phylogenetic Analysis

Phylogenetic analysis was conducted using TNT v1.5 (Goloboff and Farris, 2008), with the settings used in Longrich et al. (2018): ordered and unordered characters were used and equally weighted; continuous characters were rescaled to unity using the "nstates stand" command; basic tree searches of 2000 random addition sequence replicates were conducted with and without the parsimony ratchet; ambiguous branch support was not used; zero-length branches were automatically collapsed; and the resulting trees filtered for best score. Support measures were calculated in TNT, including Bremer supports using the BREMER.RUN script with default settings, and bootstrap using the same parsimony settings as the tree-searching analysis and default deletion percentages (50%) for 10,000 replications by following command:

RESAMPLE boot replications 10000 frequency from N;

where N depends on the numbering of the resulting tree. The ensemble consistency index (CI) and ensemble retention index (RI) were calculated using the STATS.RUN script included within TNT v1.5. For time calibration, the timescale is from Gradstein et al. (2012), and age ranges for species were downloaded from the Paleobiology Database (https://www.paleobiodb.org/).

TABLE 1. Allometric equations ($y = a \cdot x^b$) of skeletal variables. -, =, and + indicate negative allometry, isometry, and positive allometry, respectively. **Abbreviations**: **A**, allometry; **CI**, one-tailed 95% confidence interval.

x	y	R^2	p	a	b	CI (b)	A	n
humerus	skull length	0.845	<0.001	2.931	0.572	≤0.766	-	10*
	skull width	0.812	0.002	2.752	0.664	≤0.919	-	8*
	ulna/radius	0.963	<0.001	1.611	0.970	≤1.108	=	10
	mciv	0.936	<0.001	0.188	1.153	≥0.963	=	9
	pteroid	0.972	<0.001	0.102	1.170	≥1.003	+	7
	wp1	0.968	<0.001	1.827	0.972	≤1.174	=	9
	wp2	0.959	<0.001	1.523	0.974	≤1.273	=	8
	wp3	0.967	<0.001	0.374	1.241	≥1.111	+	7
	wp3 + wp4	0.975	0.002	0.268	1.372	≥1.106	+	5
	wingspan	0.974	<0.001	10.332	1.097	≥1.000	+	11
	femur	0.963	<0.001	1.025	0.904	≤0.982	-	11**
	tibia	0.910	<0.001	1.383	0.900	≤1.032	=	11
	foot	0.950	<0.001	0.722	1.038	≥0.940	=	10
	manual claw	0.964	<0.001	0.070	1.250	≥1.143	+	9
	pedal claw	0.933	<0.001	0.029	1.373	≥1.235	+	10
skull width	skull length	0.966	<0.001	1.095	0.887	≤1.000	-	8*
tibia	ulna/radius	0.911	<0.001	1.191	1.061	≥0.886	=	10
pdV-1	mtiii	0.874	<0.001	0.719	1.034	≥0.777	=	8
ulna/radius	mciv	0.928	<0.001	0.108	1.187	≥0.959	=	8
pedal claw	manual claw	0.997	<0.001	1.588	0.961	≤1.000	-	9
pdIII	pdV	0.899	0.004	2.147	0.935	≤1.726	=	6
femur	tibia	0.960	<0.001	1.305	1.002	≥0.919	=	10**
mtiii	mciv	0.878	<0.001	0.401	1.218	≥1.007	+	9
scapula	coracoid	0.641	0.031	0.469	1.142			7
tibia	fibula	0.937	0.002	0.168	1.313	≥0.945	=	6
wp1	wp2	0.986	<0.001	0.835	1.004	≥0.925	=	8

*Without specimens of *Batrachognathus volans*; **Without the holotype specimen of *Sinomacrops bondei*.

ALLOMETRIC ANALYSIS

Allometric Growth in Anurognathids

In the bivariate allometric analysis, all pairs but one show significant correlations ($p < 0.05$); 77% of these correlations have coefficients of determination (R^2) ≥0.90 and 54% ≥0.95 (Table 1). This suggests that despite the inclusion of multiple species, growth trajectories of these elements are conservative and shared by all studied anurognathids with only three exceptions. The first exception is the skull length of *Batrachognathus volans*; this plots separately to other specimens, well above the regression lines (Fig. 2A and C) and is thus proportionally longer irrespective of ontogeny (its skull width is similar to other specimens; Fig. 2B). Second, the femur length of *Sinomacrops bondei* is proportionally shorter than that of other specimens (Fig. 2L). This probably explains its unusual tibia:femur length ratio, a diagnostic trait

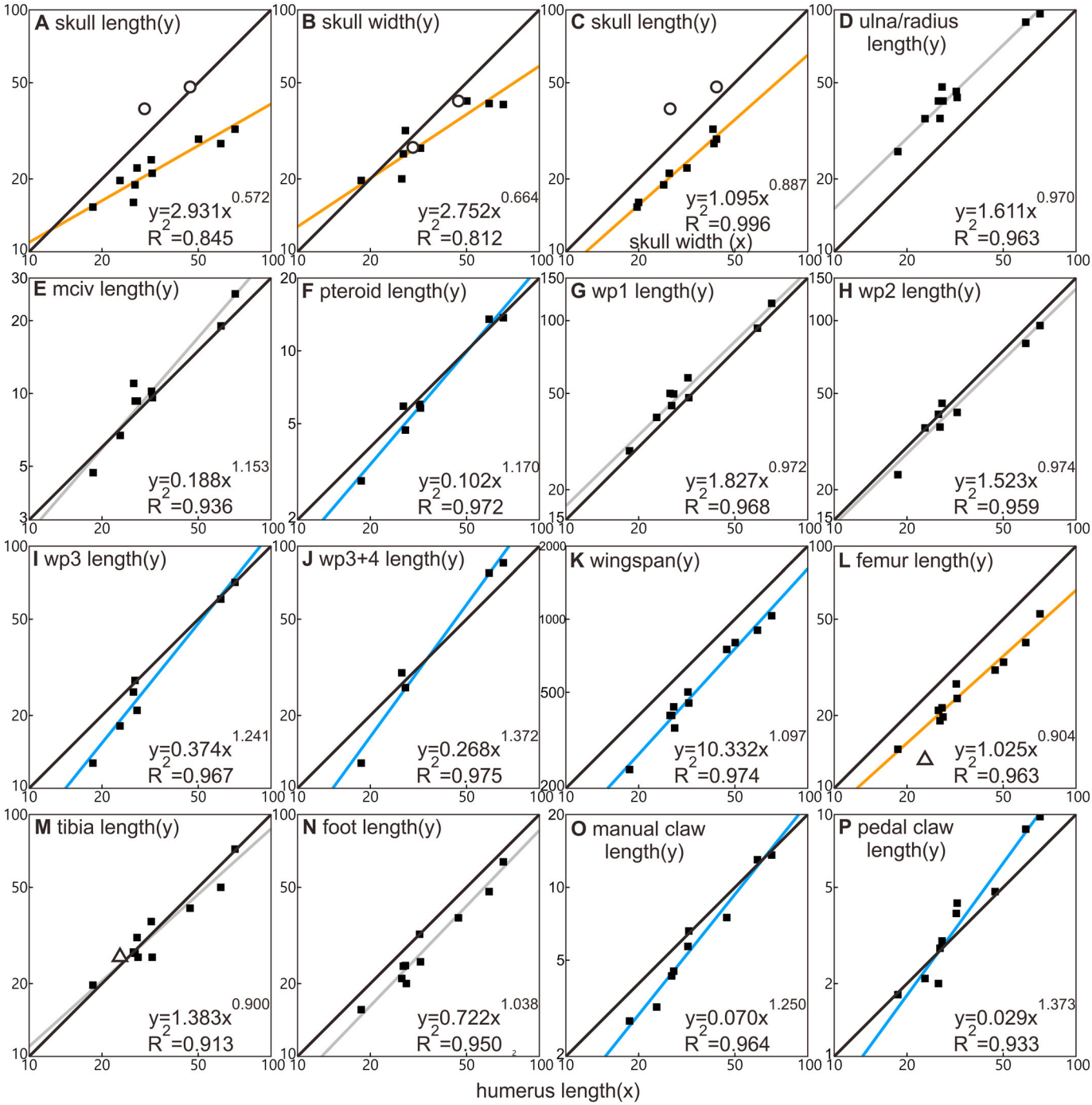

FIGURE 2. Allometric growth of various skeletal dimensions relative to humerus (**A**, **B** and **D**–**P**) and to skull width (**C**). Both x and y axes were log-transformed and the values are in millimeters, and slope of the thick black lines corresponds to isometry ($b = 1$). Trendlines of negative allometry, isometry, and positive allometry are indicated by orange, gray, and blue, respectively, in the online version of this article. In **A**–**C** and **L**–**M**, the white circles indicate specimens of *Batrachognathus volans*, and the white triangles indicate the holotype of *Sinomacrops bondei*; the black squares indicate the other anurognathids.

(Wei et al., 2021); its tibia length is similar to that of other specimens (Fig. 2M). The third exception is the scapula-coracoid pair ($p = 0.064$; Table 1), which also represents strong interspecific variation: scapula:coracoid length ratio ranges from 2 in the *Jeholopterus ningchengensis* holotype to less than 1 in *Vesperopterylus lamadongensis*.

Among the dimensions with shared growth trajectories, those from the skull have the largest deviations from isometry, with both length and width showing strong negative allometry relative to the humerus (Figs. 1A, 2A, B; Table 1). The relatively low R^2 values (0.845 and 0.812 for skull length and width, respectively) probably reflect a combination of interspecific variation and the effect of dorsal-ventral compaction commonly seen in these specimens. In addition, skull length exhibits negative allometry relative to width (Fig. 2C), suggesting that the shape of the skull becomes proportionally broader with growth.

In the limbs, only the femur shows slight negative allometry relative to the humerus, while the pteroid, both manual and pedal claws, wp3–4 and wingspan exhibit positive allometry and the remaining elements (ulna/radius, metacarpal IV and wp1–2) grow isometrically (Figs. 1A, 2; Table 1). Wingspan shows only slight positive allometry, despite relatively strong positive allometry in wp3–4, because the latter account for <10% of the wingspan. Similarly, although the pedal claw shows relatively strong positive allometry to the humerus (Figs. 1A, 2P), the growth of foot length overall is isometric (Figs. 1A, 2N).

In some cases, the recovered allometric scaling coefficients suggest allometry, but are interpreted here as evidence of isometry based on the bootstrapping results. These cases include humerus–metacarpal IV, humerus–tibia, ulna/radius–metacarpal IV, pdIII–pdV, metatarsal–metacarpal IV, and tibia–fibula (Fig. 2; Table 1). This conflict between allometric scaling coefficients and bootstrapping results probably reflects relatively higher interspecific variation in these elements (e.g., pdV:pdIII length ratio ranges from 2.1–1.5 among anurognathids), and/or the small sample size, preventing discrimination of the allometric scaling coefficient from 1 (isometry).

In the PCA, length data of scapula and coracoid were excluded from the analysis due to the strong interspecific variation detected (Table 1). *Batrachognathus volans* and *Sinomacrops bondei* were included but with respective skull length and femur length treated as missing data, given the interspecific variations in these dimensions (Fig. 2A, L) and that the other studied dimensions follow the growth trajectories in other anurognathids.

PC1 captures 95.9% of total variance with high scores for large specimens, supporting PC1 as a size factor (Table 2). The resulting allometric pattern is largely compatible with the bivariate analysis using humerus length as a body size proxy (Fig. 1). PCA recovered the humerus with only slight negative allometry, and as such, the allometric status of many skeletal variables identified by PCA (including skull length and width, manual and pedal claws, pteroid, wp3–4 and femur) is the same as that suggested by the bivariate analysis (Fig. 1). Further, in both analyses the skeletal variables rank similarly using the allometric scaling coefficients (Tables 1 and 3): pedal claw > manual claw > pteroid > metacarpal IV > wingspan > foot > wp2 > wp1 > ulna/radius > femur > tibia > skull width > skull length. The only discrepancy is the ranking of wp3–4 and pedal claw, which is wp3–4 > pedal claw in bivariate analysis and the reverse in PCA; nonetheless in both analyses the coefficient values are similar and indicate positive allometry.

Notably, the humerus allometric scaling coefficient recovered by PCA is slightly below 1 (negative allometry), unlike in bivariate analysis where it is assumed to equal 1 (isometry). In summary, our results show that for each skeletal variable bivariate analysis consistently produces higher allometric scaling coefficient values than PCA (Tables 1, 3). As a result, bivariate analysis recovered ulna/radius, wp1 and tibia with allometric scaling coefficients < 1 (albeit statistically indistinguishable from 1), whereas PCA indicates negative allometry in these dimensions. Similarly, wingspan growth is recovered as slightly positively allometric using bivariate analysis, but isometric using PCA.

TABLE 2. PC1 scores for each specimen.

Specimens	PC1 score
SMNS 81928	−1.3082
JPM-2012-001	−0.7289
IVPP V16728	−0.52567
GMV 2128	−0.44673
JZMP-04-07-3	−0.43384
NJU-57003	−0.28187
PIN 2585/4a	−0.24714
CAGS-Z070	−0.17496
BSP 1922 I 42	0.10728
PIN 52-2	0.56691
Korean specimen	0.87861
IVPP V12705	1.1134
BMNHC-PH-001311	1.4811

Biases in Diagnoses and Character Matrices

According to the allometric analysis, seven characters previously used to diagnose anurognathid taxa (see Supplemental Data 2 for the full list) are biased by allometric growth: (1) wingspan (Bakhurina and Unwin, 1995; Wang et al., 2002); (2) skull size (Lü and Hone, 2012; Lü et al., 2018); (3) skull aspect ratio (Wang et al., 2002; Lü and Hone, 2012; Lü et al., 2018), except for *Batrachognathus volans*; (4) length ratio of (femur + tibia) to humerus (Unwin and Bakhurina, 2000); (5) length ratio of humerus to femur (Kellner, 2003; Wang et al., 2005; Wei et al. 2021), except for *Sinomacrops bondei*; (6) length ratio of metacarpal IV to metatarsal I–III (Lü et al., 2018); and (7) length ratio of metacarpal IV to lower arm (Wang et al., 2002). These were omitted in the taxonomic study (below) of the new anurognathid taxon.

TABLE 3. Allometric scaling coefficients for each skeletal variable resulted from PCA. -, =, and + indicate negative allometry, isometry, and positive allometry, respectively. **Abbreviations**: **CI**, confidence interval.

Skeletal variable	b	95% CI for b	allometry
skull length	0.518	≤0.599	-
skull width	0.610	≤0.789	-
humerus	0.951	≤0.993	-
ulna/radius	0.920	≤0.973	-
mciv	1.093	≥0.948	=
pteroid	1.114	≥1.021	+
manual claw	1.193	≥1.093	+
wp1	0.943	≤0.968	-
wp2	0.944	≤1.003	=
wp3 + wp4	1.327	≥1.231	+
wingspan	1.042	≥0.996	=
femur	0.854	≤0.924	-
tibia	0.850	≤0.947	-
mtiii	0.924	≤1.041	=
pdIII	1.074	≥0.957	=
foot	0.994	≤1.062	=
pedal claw	1.292	≥1.163	+
Fibula	1.097	≥0.860	=
pdV–1	0.916	≤1.069	=
pdV–2	0.981	≤1.109	=

Further, nine characters in the character list (Supplemental Content) use length ratios that can be biased by ontogenetic variation in anurognathid proportions, including Chars. 1 (skull: humerus ratio of 0.452–0.823 except for *Batrachognathus*), 32 (pteroid:ulna ratio of 0.098–0.166), 33 (metacarpal IV:humerus ratio of 0.282–0.407), 37 (wp2:wp1 ratio of 0.796–0.915), 38 (wp3:wp1 ratio of 0.423–0.769), 39 (wp4:wp1 ratio of 0.100–0.183), 43 (femur:humerus ratio of 0.645–0.778 with the exclusion of *Sinomacrops*), 45 (fibula:tibia ratio of 0.408–0.666) and 46 (metatarsal III:tibia ratio of 0.399–0.532). Excepting *Batrachognathus* and *Sinomacrops*, which were coded using their unique length ratio for Chars. 1 and 43, respectively, specimens were assigned the ontogenetically corrected states for these characters (see Character Matrices in Materials and Methods).

SYSTEMATIC PALEONTOLOGY

PTEROSAURIA Kaup, 1834
ANUROGNATHIDAE Kuhn, 1937
CASCOCAUDA RONG gen. et sp. nov.
(Figs. 3–6, S1)

Holotype—The holotype is NJU-57003, preserving a well-articulated and nearly complete skeleton with extensive preserved soft tissues (Figs. 3–6, S1). The specimen comprises two fragmented slabs (main slab and counter slab), which are housed in Nanjing University, Nanjing, China.

Etymology—The generic name is composed of the Latin 'cascus' meaning 'ancient, primitive', and 'cauda' meaning 'tail.' The specific name is from Chinese character róng (绒), as used in the phrase máo róng róng, meaning 'a fluffy appearance,' which refers to the extensive integumentary covering (Yang et al., 2019).

Locality and Horizon—The holotype was recovered from Mutoudeng, Qinglong County in Hebei Province, China, from the Middle—Upper Jurassic Tiaojishan Formation (Xu et al., 2016).

Diagnosis—A new anurognathid pterosaur that differs from other anurognathids by the following combination of diagnostic features: at least 20 caudal vertebrae with elongate zygapophyses and chevrons (different from *Jeholopterus*, *Anurognathus*, *Dendrorhynchoides*, and *Vesperopterylus*), scapula slightly longer than coracoid with a length ratio of 1.2 (different from *Luopterus*, *Jeholopterus*, and *Vesperopterylus*), second phalanx of pedal digit V curved (different from *Luopterus* and *Jeholopterus*), long and thin teeth with distal curvature (different from *Anurognathus* and *Vesperopterylus*), humerus subtriangular deltopectoral crest (different from *Batrachognathus* and *Sinomacrops*) and skull wider than long (different from *Batrachognathus*).

Remarks—The differences in many skeletal proportions among anurognathids are related to growth based on their shared allometry. However, NJU-57003 is unique in two skeletal proportions of taxonomic significance and several non-ratio diagnostic traits (see above), which warrants the erection of a new taxon notwithstanding its immaturity. Further, excluding the growth-related characters in the diagnoses of existing anurognathid species, the unbiased characters are diagnostic and therefore the seven species previously erected remain valid. In addition to the eight established species, CAGS-Z070 appears to represent another unrecognized species yet to be formally named. It has been referred to the genus *Jeholopterus* (Kellner et al., 2010) but differs from the holotype

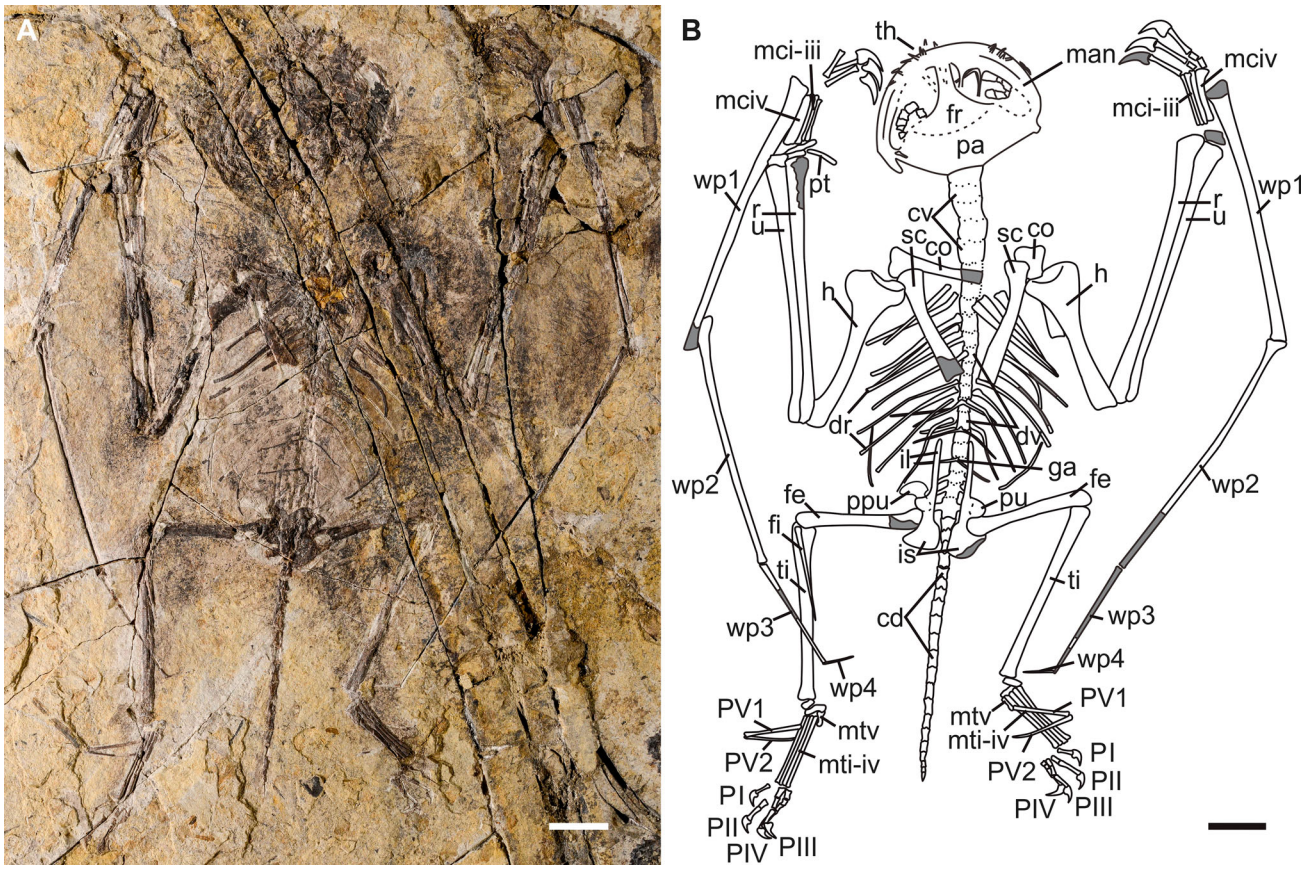

FIGURE 3. Holotype specimen of *Cascocauda rong* (NJU-57003). **A**, overview of the main slab; **B**, line drawing of the holotype with skeletal element identification. Dark gray shading represents partial losses of original bones inferred from remaining impressions. Scale bars equal 10 mm.

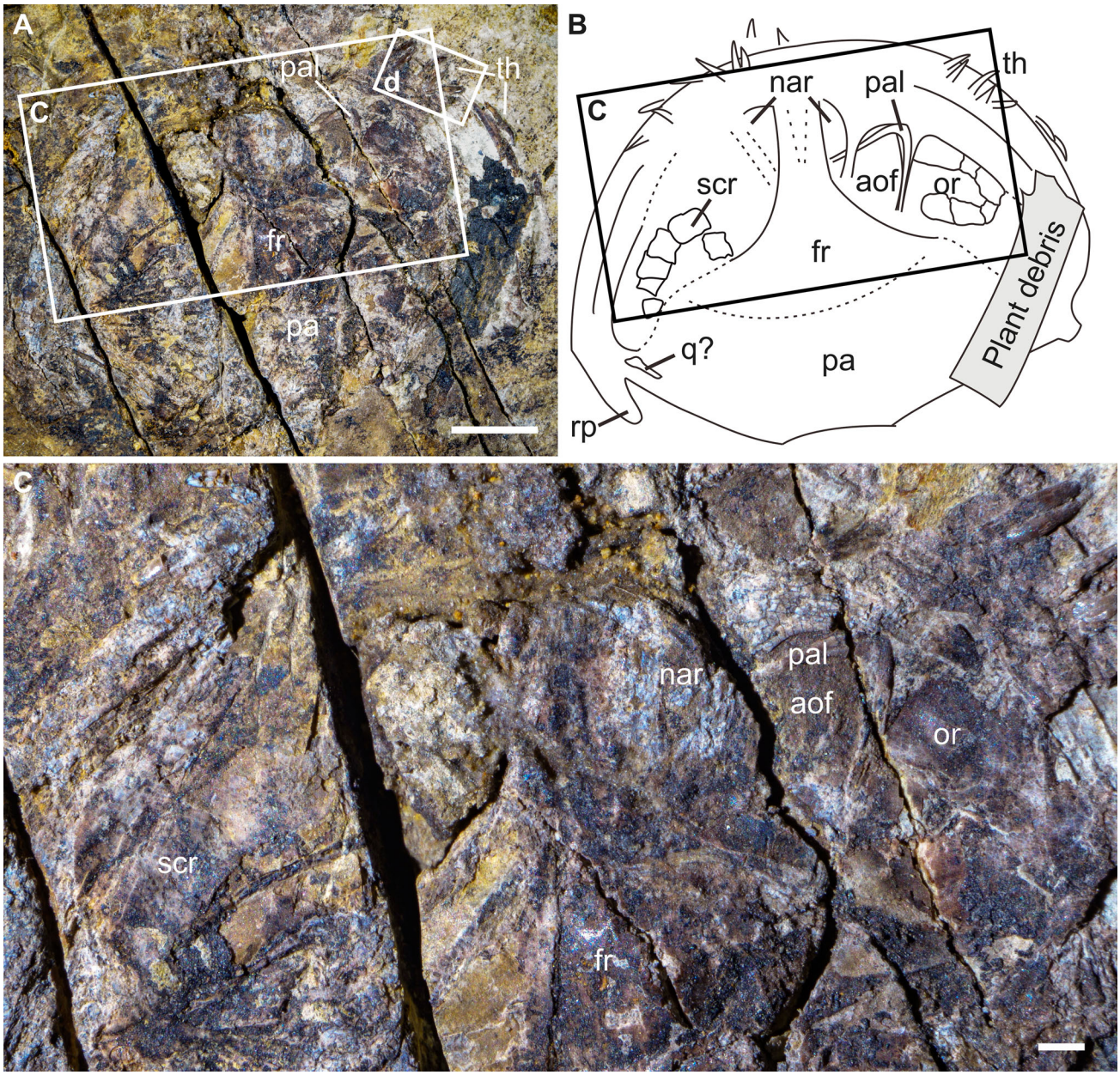

FIGURE 4. Close-up photographs and line drawings of the skull of holotype specimen of *Cascocauda rong* (NJU-57003). **A**, **B**, short and broad skull with widely spaced teeth. **C**, close up of the anterior portion of the skull showing separated naris and antorbital fenestrae. Scale bars equal 5 mm (**A**) and 1 mm (**C**).

specimen of that taxon in scapula:coracoid length ratio (1.1 rather than 2), tooth morphology (striated rather than smooth texture, and short teeth rather than both long and short teeth), pteroid shape (straight rather than curved; although this could be due to the preserved orientation in which a curved element can appear straight) and pdV-2 shape (curved rather than straight).

Description

The holotype specimen of *Cascocauda rong* has a wingspan of 434 mm and is preserved in dorsal view on the main slab, with wings folded on both sides of the body and hindlimbs flexed (Figs. 3, S1). The skeleton is near complete and well-articulated, with extensive preservation of pycnofibers and wing membranes.

Ontogenetic Status—The specimen represents a juvenile based on the unfused articular bones, such as carpals, scapula, and coracoid (Fig. 5E, F), and the pitted and rough articular surfaces of limb bones (Fig. 5C, D) indicative of incomplete ossification.

Skull—The skull is wider than long (22.2 mm long and 31.7 mm wide) with a typical anurognathid frog-like jaw (Figs. 4A, B and S2). Most of the cranial bones are highly compressed and poorly defined, with frontal, palatine, teeth and the retroarticular process being barely discernible. On the right side, two processes extending from the anterior portion of the upper jaw towards the frontal probably represent the ascending processes

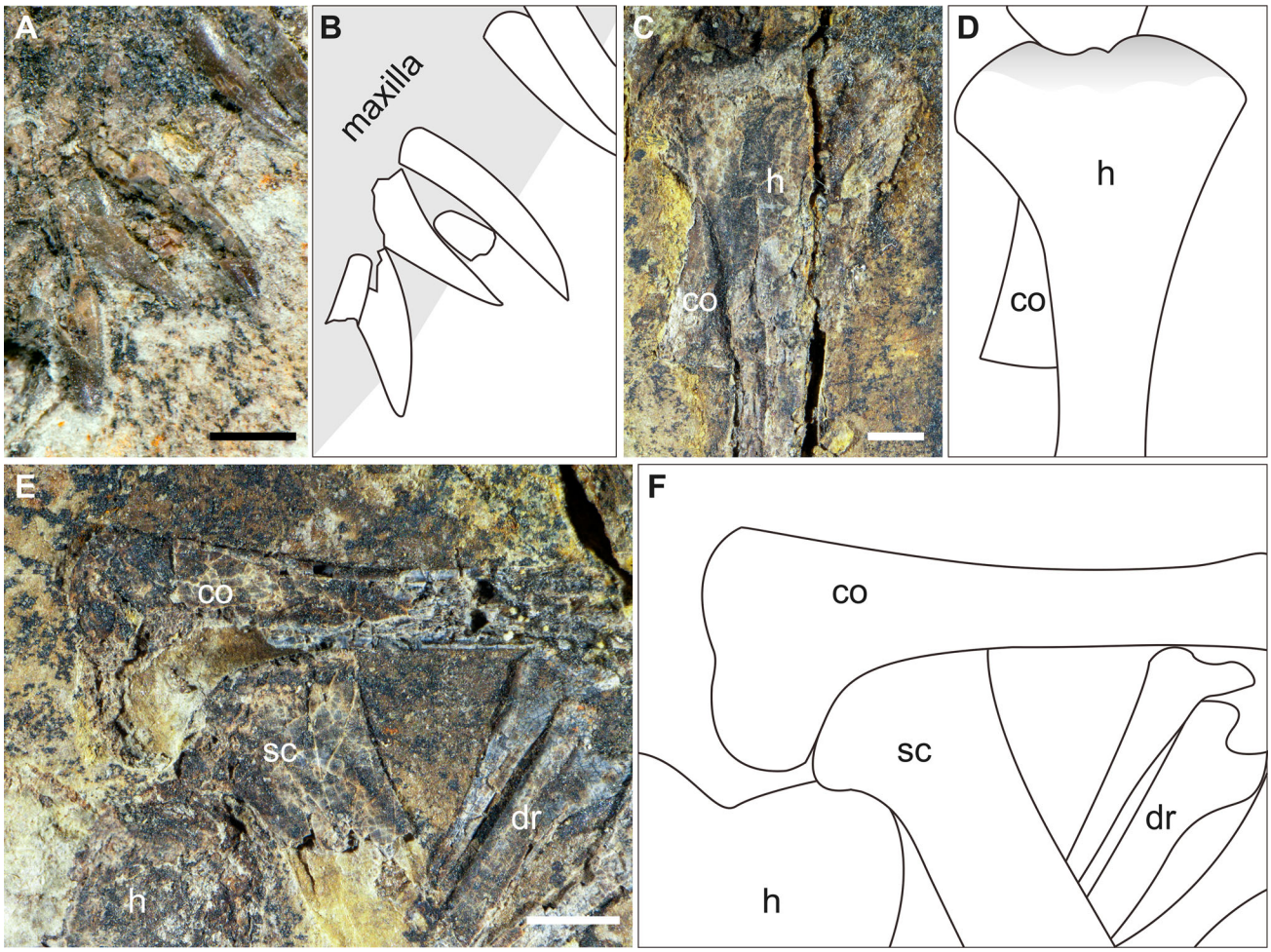

FIGURE 5. Close-up photographs and line drawings of holotype specimen of *Cascocauda rong* (NJU-57003). **A**, **B**, long, thin teeth with distal curvature. **C**, **D**, humerus with subtriangular deltopectoral crest and pitted and rough surface at proximal end (shaded area in **D**). **E**, **F**, unfused scapula and coracoid. Scale bars equal 1 mm (**A**) and 2 mm (**C** and **E**).

of the maxilla and the jugal/nasal, respectively; these separate the naris, antorbital fenestra and orbit (Figs. 4C and S2). On the left, the ascending process of the maxilla is partially preserved and part impression, while the ascending processes of the jugal/nasal are not preserved (Figs. 4C and S2). Nineteen widely spaced teeth are visible; these are 2.2–2.7 mm long, ~0.5 mm wide at the midpoint and distally curved with smooth surfaces (Fig. 5A, B).

Vertebral Column—The cervical, dorsal, and sacral vertebrae are crushed or partially covered, so the exact number of vertebrae is uncertain (Fig. 3). The neck is represented by short and robust cervical vertebrae. No evidence of cervical ribs is preserved, suggesting they were highly reduced or absent. At least ten dorsal vertebrae are preserved. Dorsal ribs are straight or slightly curved in the anterior portion of the body, while the more posterior ribs are distinctly curved posteriorly. Sacral vertebrae are short, broad, and articulated with the caudal vertebrae, and bear posterolaterally directed ribs and/or transverse processes. Three rows of gastralia are preserved and become progressively shorter caudally. Caudal vertebrae are well-preserved and articulated. Although the boundaries between several caudal vertebrae are obscured by compression, there are at least 20 vertebrae with a total length of 42 mm (Fig. 6A). A single caudal vertebra is ~2 mm long at the base of the tail, and becomes more elongate posteriorly, reaching a maximum length of 3.4 mm near the midpoint, and then shortens towards the distal tip. Elongate zygapophyses and chevrons (exposed by the absence of some caudal vertebrae) are best preserved in the middle portion of the tail, where they are at least twice the length of the vertebral centrum (Fig. 6A, B); the paired appearance of chevrons probably reflects superposition of vertebrae rather than bifurcation of the structure.

Pectoral Girdles—The scapulae are unfused to, and longer than the slightly curved coracoids. They are preserved in articulation on the left, where they meet in a 'V' shape at an angle of ~60° (Figs. 3, 5E, F).

Forelimbs—The humerus is robust, with a sub-triangular deltopectoral crest (Fig. 5C, D). The shaft of the humerus is slightly curved and the articular surfaces are pitted and rough (Figs. 3, 5C, D). Ulna and radius are both straight and significantly longer than the humerus, only slightly shorter than the first wing phalanx, and subequal in length to the second wing phalanx (Fig. 3). No epiphysis is discernible due to extensive fragmentation during burial. Carpals are poorly preserved and difficult to discern individually. The pteroid is short,

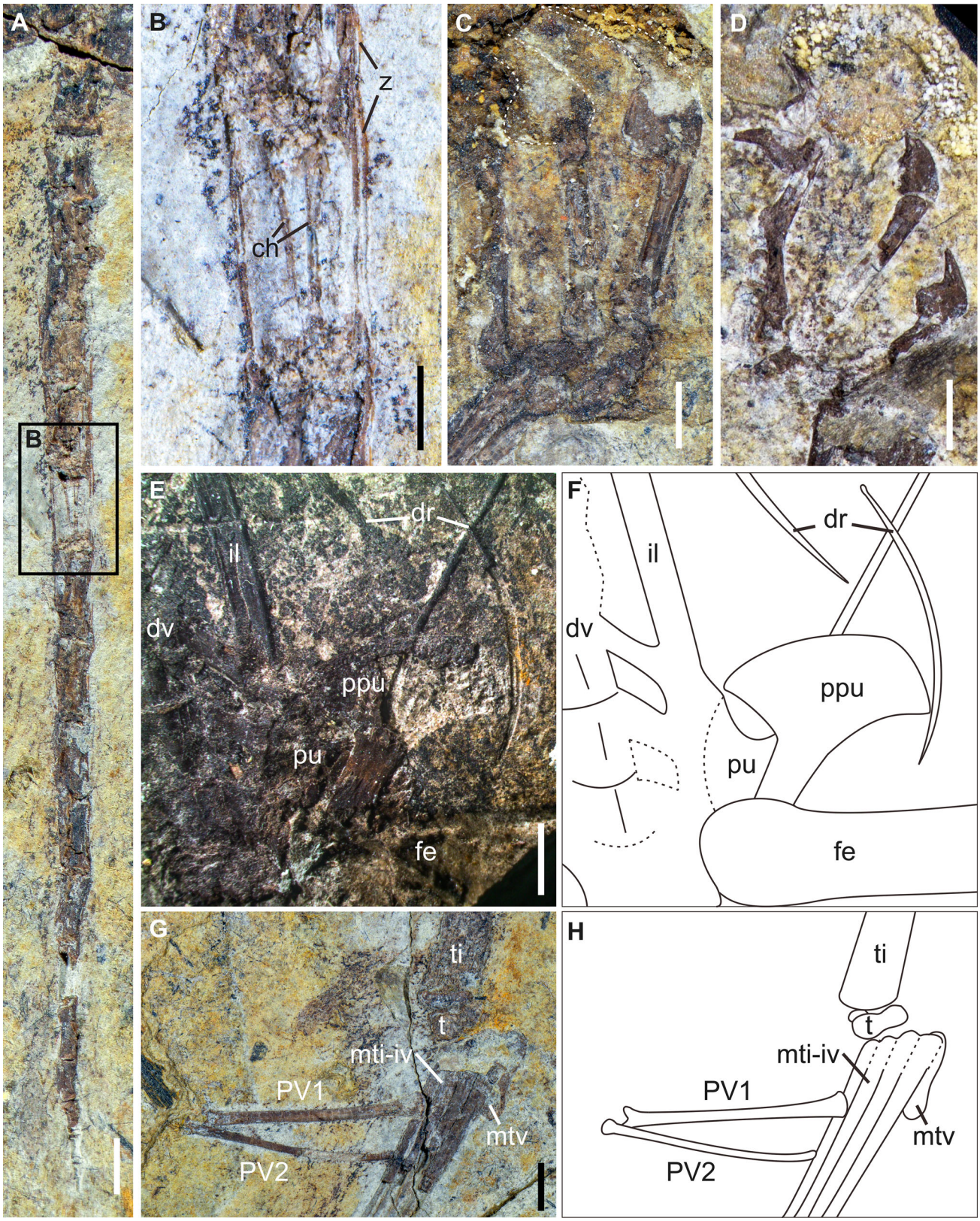

FIGURE 6. Close-up photographs and line drawings of the holotype specimen of *Cascocauda rong* (NJU-57003). **A**, **B**, completely preserved tail with elongated rod-like structures interpreted as zygapophyses and chevrons. **C**, Large curved manual claws. **D**, curved pedal claws (counter slab). **E**, **F**, pelvic girdle (counter slab) showing a long and slender iliac anterior process and a fan-shaped prepubis, and in articulation with the left femur (impression; original bone preserved on the main slab). **G**, **H**, ankle region showing unfused tibia and tarsal, metatarsals i–v similar in robustness, and pedal digit V with a long and gently curved phalanx 2. Scale bars equal 2 mm (**A**, **C**–**E**, and **G**) and 1 mm (**B**).

curved, and blunt at the distal end. The four metacarpals are subequal in length and less than one quarter the length of the radius. The wing metacarpal is much more robust than the other three. The manual claws are strongly curved, sharp and similar in shape to the pedal claws, but the manual claws are larger and more robust (Fig. 6C, D). The wing consists of four phalanges that exhibit a rapid reduction in length proceeding distally, although the lengths of the first two phalanges are similar (Fig. 3).

Pelvic Girdles—The bones of the pelvic girdle are articulated with the hindlimb (Figs. 3, 6E, F) and although crushed, are separated, indicating an unfused state. The ilia have long and slender anterior processes, but the shape of the posterior processes is unclear. The ischia are broad plates that approach each other closely at the posterior end. The shape of the pubis is difficult to discern. The left prepubis bears a distinct proximal shaft and an asymmetrically fan-shaped distal portion (Fig. 6E, F).

Hindlimbs—The femur is straight and oriented nearly perpendicular to the vertebral column. The fibula is not fused to the tibia, tapering out at less than half the length of the tibia. Metatarsals I–IV are straight and parallel to each other with nearly equal lengths. The fifth metatarsal is slightly more robust but significantly shorter than metatarsals I–IV. The phalangeal formula is 2-3-4-5-2. The first digit of the pes is not reversed, and in pedal digits II–IV the penultimate phalanges are longer than the more proximal phalanges (Figs. 3, 6D). Pedal digit V consists of two long phalanges, of which the first phalanx is robust and straight, while the second is slender and slightly curved (Fig. 6G, H).

PHYLOGENETIC ANALYSIS

By using ontogenetically corrected coding and treating only *Cascocauda* and *Anurognathus* as having separated naris and antorbital fenestrae (with the character coded as unknown for all other specimens; Supplemental Data 3), our analysis produced a single most parsimonious and fully resolved tree (Fig. 7), with 850.283 steps, consistency index (CI) of 0.442 and retention index (RI) of 0.708. Most major clades are recovered, among which the Anurognathidae, supported by 42 synapomorphies (see Supplemental Results for details), is placed as the sister group of Breviquartossa. Within Anurognathidae, *Cascocauda rong* is the sibling group to (*Batrachognathus volans* + *Sinomacrops bondei*), which together form the Batrachognathinae (sensu Kellner et al., 2010). Alongside Batrachognathinae, the Anurognathinae (sensu Wei et al., 2021) comprises all other anurognathids. The number of synapomorphies supporting each internal node of Anurognathidae varies from 3 to 13 (Supplemental Results). Bremer support and bootstrap scores indicate high stability (>1 for the former and over 50 for the latter) for Anurognathidae, Batrachognathinae, and *Batrachognathus volans* + *Sinomacrops bondei* (Fig. S3). Anurognathinae and the clades within are less stable: only two clades, (*Dendrorhynchoides* + *Anurognathus* + (*Vesperopterylus* + (*Jeholopterus* + CAGS-Z070))) and (*Jeholopterus* + CAGS-Z070), have Bremer support scores of 1, and only the clade (*Jeholopterus* + CAGS-Z070) has a bootstrap score higher than 50.

Ontogenetically uncorrected coding (Supplemental Data 4) produced an identical tree topology with a slightly longer tree length (852.302 steps) and similar Bremer support and bootstrap

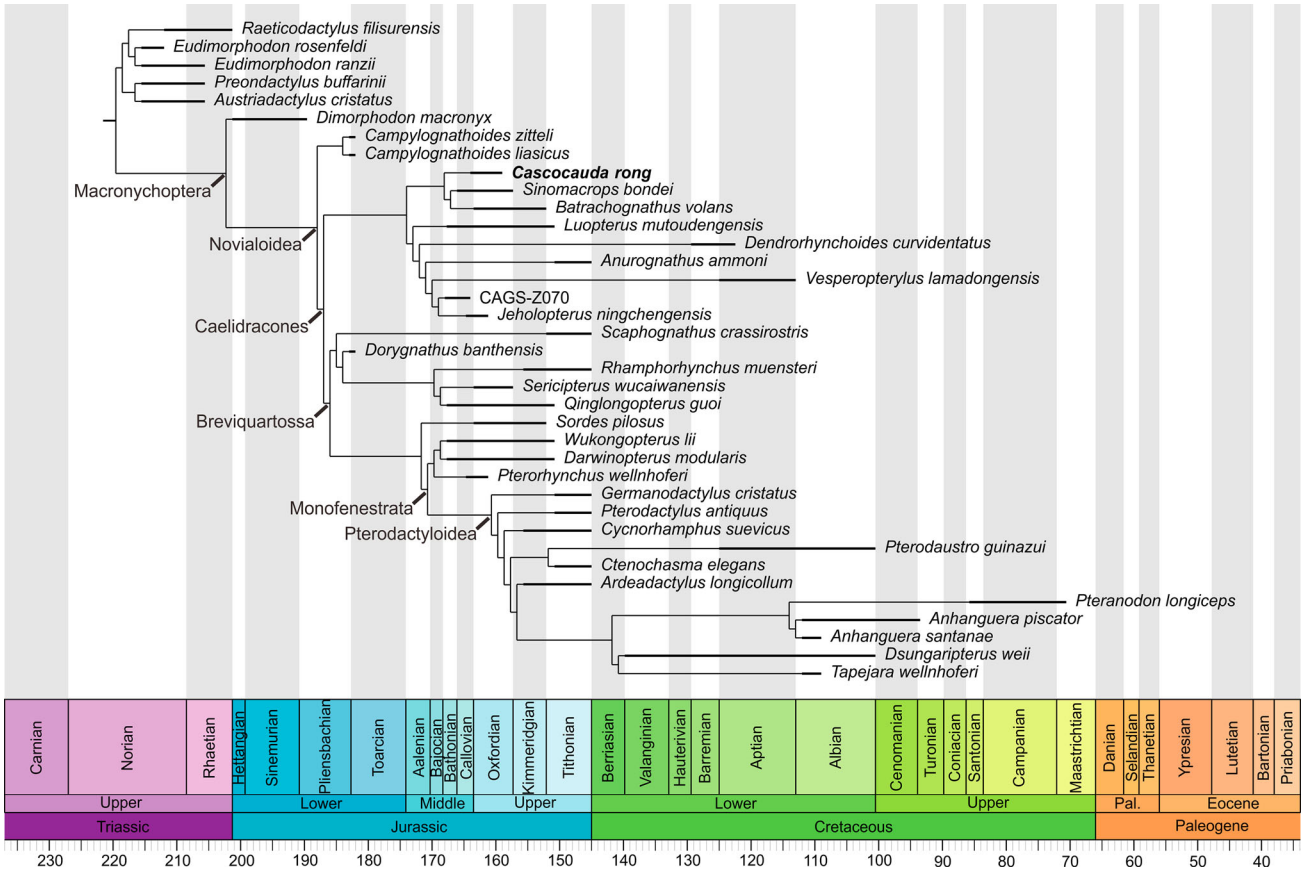

FIGURE 7. Single most parsimonious trees recovered from the phylogenetic analysis using ontogenetically corrected coding.

scores (Fig. S4A). The phylogenetic analysis is thus subject to limited allometric growth bias, probably because (1) the number of biased characters is small compared with the total number of informative characters, and (2) growth-related variations are coded as continuous characters and thus caused relatively small step changes (always <1 by each character) compared with the informative discrete characters.

We also ran the analysis using ontogenetically corrected coding but under a different scenario for the configuration states of the naris and antorbital fenestra (Supplemental Data 5), i.e., treating *Cascocauda* as separated, *Batrachognathus volans*, *Sinomacrops bondei*, and CAGS-Z070 as confluent (Wei et al., 2021), and the rest of anurognathids as unknown. The analysis produced an identical tree topology to the original and 'ontogenetically uncorrected' analyses, although with an even longer tree length (853.227 steps) than the latter, and similar Bremer support and bootstrap scores (Fig. S4B). The Bremer support for Batrachognathinae was reduced to 1, probably because the analysis recovered the configuration of the naris and antorbital fenestra of Batrachognathinae as ambiguous (Fig. S5).

DISCUSSION

Allometry-related Biases in Anurognathid Systematics

Our analysis demonstrates that anurognathids share the same growth trajectory in most skeletal dimensions and that seven characters in existing anurognathid diagnoses relate to allometric growth rather than interspecific variations. Similar studies of other pterosaur clades, on skeletal proportional changes during growth, have suggested or led to taxonomic revisions, including synonymization of multiple species based on shared growth curves (e.g., Bennett, 1995, 1996, 2007b, 2013; Jouve, 2004) and recognition of the outliers of the curves as separate taxa (e.g., Bennett, 2006; Vidovic and Martill, 2014). In Anurognathidae, however, excluding the biased characters, the rest of the diagnosis remains sufficient to discriminate among existing species, which are thus considered valid here. Our analysis also recognizes two outliers among the shared growth trajectories, i.e., the proportionally longer skull of *Batrachognathus volans* and the shorter femur of *Sinomacrops bondei*, further supporting the validity of these two species.

Concerning phylogenetic analysis, although the detected allometry-related biases have not affected tree topology in the present study, they might have a more discriminatory effect if the number of informative characters (and consequently synapomorphies) is small. In pterosaur phylogenies, nodes usually have few supporting characters (Lü and Hone, 2012); this is particularly true for interpretations of anurognathid systematics that have relied on limited available information (see discussion in Hone [2020] and Wei et al. [2021]). For instance, the position of *Anurognathus* as the earliest-diverging member of Anurognathidae is typically supported by a single character: the proportional size of the humerus compared with the femur (Kellner, 2003; Wang et al., 2005). According to our results, however (Fig. 2L), this character arises from ontogenetic rather than phylogenetic variation, and thus the proposed phylogenetic position is not valid.

Phylogeny of Anurognathids

The phylogenetic position of Anurognathidae and the interrelationships of anurognathid taxa have historically been contentious. Six hypotheses have been proposed for the position of Anurognathidae, where the clade is viewed as: the earliest-diverging pterosaur group (e.g., Kellner, 2003; Lü and Ji, 2006; Bennett, 2007a; Wang et al., 2008; Lü et al., 2018); the sister-group of Novialoidea (Unwin, 2003b; Lü et al., 2010); the sister-group of Breviquartossa (Viscardi et al., 1999; Britt et al., 2018; Dalla Vecchia, 2019); belonging to the Scaphognathidae (Vidovic and Martill, 2018); the sister-group of Pterodactyloidea (Dalla Vecchia, 2009; Andres et al., 2010, 2014); or a basally branching monofenestratan group (Wei et al., 2021). Interspecific relationships within Anurognathidae are also inconsistent, with numerous different topologies having been proposed (Kellner, 2003; Unwin, 2003a; Lü and Ji, 2006; Andres et al., 2014; Wang et al., 2017; Lü et al., 2018; Vidovic and Martill, 2018; Wei et al., 2021).

Given ongoing discoveries of new anatomical traits and species of anurognathids, particularly in recent years (e.g., Jiang et al., 2015; Lü et al., 2018; Hone, 2020; Wei et al., 2021), we compare our phylogenetic results primarily with the most recent and species-inclusive phylogenetic study by Wei et al. (2021), albeit with reference to others.

Our phylogenetic placement of Anurognathidae, outside Monofenestrata and as the sister-group of Breviquartossa (Fig. 7), differs from the suggestion by Wei et al. (2021) that the clade is the basal-most branch in Monofenestrata. One key factor is that we code anurognathids as either having separate external nasal and antorbital fenestrae (*Cascocauda* and *Anurognathus*) or unknown (other anurognathids), whereas the group was considered to have a confluent nasoantorbital fenestra (a feature typical of the Monofenestrata and coded as present in *Batrachognathus*, *Sinomacrops* and CAGS-Z070) by Wei et al. (2021). This difference in reconstructions arises from the poor preservation of the ascending processes of the maxilla, either undiscernible or isolated from the maxilla, that, if present, would have separated the naris and antorbital fenestra (Andres et al., 2010; Wei et al., 2021). The newly described holotype of *Cascocauda rong*, however, preserves two distinct processes rising from the anterior portion of the upper jaw towards the frontal (Fig. 4C), which are most likely the ascending processes of the maxilla and jugal/nasal, respectively. The absence of the ascending process of the maxilla in holotypes of *Batrachognathus* and *Sinomacrops* and specimen CAGS-Z070 (Wei et al., 2021) is not necessarily evidence for its anatomical absence but that this structure is fragile and prone to displacement during fossilization. As such, we consider that available evidence supports the traditional view of separate nasal and antorbital fenestrae in anurognathids (Bennett, 2007a; Hone, 2020).

If we code *Batrachognathus*, *Sinomacrops* and CAGS-Z070 as having a confluent nasoantorbital fenestra following Wei et al. (2021), and code only *Cascocauda* as having separate external naris and antorbital fenestrae and the rest as unknown, the resulting tree topology is identical to that produced by our original coding (Fig. S4B). Further, our phylogenetic placement of Anurognathidae is consistent with the position proposed by Viscardi et al. (1999), Britt et al. (2018) and Dalla Vecchia (2019); all coded the confluent nasoantorbital fenestra as present or unknown. These results further support the position of the Anurognathidae outside Monofenestrata as a sister-group of Breviquartossa and suggest that except for the configuration of the external naris and antorbital fenestrae, anurognathid anatomy is non-monofenestratan.

In terms of relationships within Anurognathidae, our results are largely congruent with Wei et al. (2021) in placing *Batrachognathus* and *Sinomacrops* as a clade and members of Batrachognathinae (with the inclusion of *Cascocauda* in the present study), placing the other anurognathids as Anurognathinae and recognizing the clade (*Anurognathus* + *Vesperopterylus* + *Jeholopterus*). Only two discrepancies occur, namely whether *Luopterus* or *Dendrorhynchoides* is the sister group to the clade (*Anurognathus* + *Vesperopterylus* + *Jeholopterus*) and relationships within the latter clade.

Wei et al. (2021) placed *Luopterus* as sister to the clade (*Anurognathus* + *Vesperopterylus* + *Jeholopterus*) based on the synapomorphy of a straight last phalanx of pedal digit V. However, this

phalanx is described as curved in both the holotype (Wellnhofer, 1970) and the referred specimen (Bennett, 2007a) of *Anurognathus*, yet coded as straight by Wei et al. (2021). Our analysis, on the basis of six synapomorphies (see Supplemental Results for details), recovered *Dendrorhynchoides* as more closely related to the clade (*Anurognathus* + *Vesperopterylus* + *Jeholopterus*), which together constitute a clade containing all short-tailed anurognathids, i.e., having fewer than 15 caudal vertebrae with disk-like morphology and short zygapophyses, and tail: humerus length ratio < 0.5.

Interestingly, according to our results, this clade of short-tailed anurognathids is immediately preceded by *Luopterus* with an elongated tail (tail:humerus length ratio of 0.67), which is further preceded by other long-tailed species with much longer tails (tail:humerus length ratio of 1.47 for *Batrachognathus volans*, 1.50 for *Cascocauda rong* and >2 for *Sinomacrops bondei*). Although positive allometric growth in the tail has been observed in *Pterodaustro* (Codorniú, 2007) and *Kunpengopterus* (Jiang et al., 2021), i.e., the tail becomes proportionally longer during ontogeny, this is probably not the case here. For instance, *Luopterus* has a similar humerus length (near isometry to body size in growth) to *Cascocauda*, but its tail is less than half as long as the latter; compared with *Sinomacrops*, *Luopterus* has a longer humerus and yet a much shorter tail length. The observed difference in tail length is therefore best explained as interspecific variation. The stepwise shortening of the tail from the Batrachognathinae to *Luopterus* and then to the clade (*Dendrorhynchoides* + *Anurognathus* + *Vesperopterylus* + *Jeholopterus*) probably reflects a general evolutionary trend of tail reduction in Anurognathinae.

Wei et al. (2021) recovered a sister-group relationship between *Anurognathus* and *Vesperopterylus* based on one synapomorphy: the complete loss of mid-cervical ribs. Although this trait characterizes *Anurognathus* and *Vesperopterylus* and has been included in our character matrix (Char. 202), our analysis found *Jeholopterus* to be more closely related to *Vesperopterylus* than *Anurognathus* based on four synapomorphies (see Supplemental Results for details). Among these four synapomorphies, while the number of teeth may be uncertain from preservational bias (loss or covered by other bones or matrix), *Vesperopterylus* and *Jeholopterus* share (1) the length to mid-width ratio of 0.9 for the third phalanx of pedal digit IV (2.3 in *Anurognathus*), (2) distinctly curved dorsal ribs in the anterior portion of the body (straight ribs in *Anurognathus*) and (3) robust first phalanx of pedal digit V (absent in *Anurognathus*). The latter two traits were not included in the analysis by Wei et al. (2021), but had been noted previously by Hone (2020), probably leading to the different results.

Support for relationships within Anurognathidae (especially Anurognathinae) will improve with incorporation of additional diagnostic features following future discovery of new specimens.

Ontogeny and Evolution of Anurognathids

The gross morphology—and presumably ecology—of anurognathids varies little both in space, across much of Eurasia (known at least from Germany, Kazakhstan, China, and North Korea) and time, over an interval of >40 million years (Unwin et al., 2000; Bennett, 2007a; Hone, 2020). They are widely interpreted as having been specialized aerial insectivores active in low light conditions based on their anatomy, including a frog-like large gape and sharp isodont dentition (Bennett, 2007a; Ősi, 2011; Hone, 2020), small size, deep wing with curved wingtip, short flexible tail (Bennett, 2007a; Ősi, 2011; Hone et al., 2015; Hone, 2020) and large eyes (Bennett, 2007a; Lü et al., 2018). Limited variation among anurognathids does, however, suggest adaptations to slightly different niches. For example, variations in the number and shape of teeth indicate different prey types (Wang et al., 2002); the reversed first toe in some anurognathids suggests enhanced gripping ability, and by extension arboreality (Lü et al., 2018); variations in the proportions of scapula and coracoid and the shape of the humerus deltopectoral crest reflect different musculature constructions and thereby flight styles (Frey et al., 2003; Hone, 2020); and reduction of the tail suggests reduction of drag, leading to higher maneuverability during flight (Evans and Thomas, 1992; Bennett, 2007a).

Our recovered allometric growth pattern suggests that the lifestyle of anurognathids changed very little in ontogeny as well as through space and time. The (near-)isometric growth in most of the wing elements and wingspan (Fig. 1) indicates that juvenile anurognathids, as small as only 0.24 m in wingspan, have very similar wing shape and relative size to adults. This indicates precocial flight capability, as has been suggested for many other pterosaurs with similar isometric growth (e.g., Unwin, 2005; Bennett, 2017; Unwin and Deeming, 2019; Hone et al., 2020; Naish et al., 2021). Given the faster (cubic) increase in body mass than isometric growth of the skeletal lengths and (squared) increase of wing area, juveniles may have had lower wing loading than adults and therefore different flight performance (Hone et al., 2020). This difference, however, may have been relatively small due to the overall low body mass and could have been offset at least partially by increasing pneumaticity during growth (Schepelmann, 1990; Wedel, 2003; Benson et al., 2012; Hone et al., 2020). Further, rather than reflecting a different flight style, a lower wing loading in juveniles may reflect foraging with a reduced flight cost (Shaw, 2011). Indeed, both juveniles and adults shared a suite of characters that would have allowed slow and highly maneuverable flight, critical for aerial insectivores, including a deep wing chord, curved wingtips, a flexible tail and likely voluntarily flexed interphalangeal joints (Unwin, 2005; Bennett, 2007a; Witton, 2008; Hone et al., 2015).

The strong negative allometry in both skull length and width (Figs. 1, 2A, B) confirms Bennett's (2007a) suggestion that the skull became smaller relative to body size during growth. Although this is common among vertebrates from strong negative allometry of brain growth (Dodson, 1975), this is not seen in at least some other pterosaurs (Bennett, 2006; Hone et al., 2020). In the case of anurognathids, it may arise from specialization on a particular size class of prey items (i.e., insects) during ontogeny, which is consistent with the stability through ontogeny of anurognathid feeding-related characters of the skull (Ősi, 2011).

Further, the robust and sharply curved manual and pedal claws of anurognathids are well adapted for quadrupedal climbing on vertical surfaces (Bennett, 1997; Unwin, 2005; Hone, 2020); the observed strong positive allometry in these elements (Figs. 1, 2O, P) probably reflects retention of climbing despite increasing bodyweight. This is consistent with other evidence for a predominantly arboreal lifestyle, including the unique, highly compact resting posture observed in both juveniles and adults, presumably for concealment in trees (Bennett, 2007a; Hone, 2020), small size (Hone, 2020) and co-occurrence of tree-dwelling animals indicative of a forest environment (Chen et al., 2019).

The retention of the juvenile lifestyle into adulthood by anurognathids may have led to their highly conserved morphology. Most other pterosaurs (Bennett, 2017) and many other reptiles (Werner and Gilliam, 1984) exhibit distinct ontogenetic niche shifts, and occupy different ecological niches to support larger body size during growth. As such, many aspects of their ecomorphology change significantly during growth, and their adult traits, divergent from plesiomorphic juvenile traits, become exaggerated in the process. In contrast, the specialized and consistent lifestyle of anurognathids during ontogeny may have caused retention of plesiomorphic juvenile traits, such as their characteristic large eyes, short skull and small size. Consequently, this may have restricted anurognathid morphospace and prevented

further morphological divergence by stabilizing selection, as has been hypothesized for some closely related cryptic species of modern bats (Mayer and Helversen, 2001).

CONCLUSION

Allometric analysis on 23 skeletal dimensions from the skull, pectoral girdle and limbs of 13 anurognathid specimens reveals an ontogenetic trajectory for this clade that affects a minority of characters that have been used to assess their taxonomy and phylogenetic position. Excluding the ontogeny-related characters, a new taxon, *Cascocauda rong* gen. et sp. nov., is erected, which displays clear evidence for separated external naris and antorbital fenestrae. Phylogenetic analysis on an ontogenetically corrected dataset supports the hypothesis that Anurognathidae is sister of Breviquartossa, and that there was a general trend of tail reduction in the family. The recovered allometric growth pattern suggests little change through ontogeny in their lifestyle as arboreal, aerial insectivores and perhaps even a consistent prey size. This specialized and ontogenetically consistent lifestyle may have retained plesiomorphic juvenile traits to later ontogeny, and confined anurognathids in a certain area of morphospace despite their broad geographic and temporal distribution.

ACKNOWLEDGMENTS

We thank Q. Ji, S. Ji and H. Huang for access to specimen CAGS-Z070 and N. MacLeod for suggestions. This work is supported by the National Natural Science Foundation of China (41688103 and 41672010) and Strategic Priority Research Program (B) of the Chinese Academy of Sciences (XDB26000000) to B.J., and the China Scholarship Council (No. 201906190142) and the program A for Outstanding PhD candidate of Nanjing University (202002A028) to Z.Y. We also thank the referees and Editor for their comments which helped improve the manuscript.

ORCID

Zixiao Yang http://orcid.org/0000-0002-5535-0652

LITERATURE CITED

Andres, B., J. M. Clark, and X. Xu. 2010. A new rhamphorhynchid pterosaur from the Upper Jurassic of Xinjiang, China, and the phylogenetic relationships of basal pterosaurs. Journal of Vertebrate Paleontology 30:163–187.

Andres, B., J. M. Clark, and X. Xu. 2014. The earliest pterodactyloid and the origin of the group. Current Biology 24:1011–1016.

Bakhurina, N. N., and D. M. Unwin. 1995. A survey of pterosaurs from the Jurassic and Cretaceous of the former Soviet Union and Mongolia. Historical Biology 10:197–245.

Bennett, S. C. 1995. A statistical study of *Rhamphorhynchus* from the Solnhofen Limestone of Germany: year-classes of a single large species. Journal of Paleontology 69:569–580.

Bennett, S. C. 1996. Year-classes of pterosaurs from the Solnhofen Limestone of Germany: taxonomic and systematic implications. Journal of Vertebrate Paleontology 16:432–444.

Bennett, S. C. 1997. The arboreal leaping theory of the origin of pterosaur flight. Historical Biology 12:265–290.

Bennett, S. C. 2006. Juvenile specimens of the pterosaur *Germanodactylus cristatus*, with a review of the genus. Journal of Vertebrate Paleontology 26:872–878.

Bennett, S. C. 2007a. A second specimen of the pterosaur *Anurognathus ammoni*. Paläontologische Zeitschrift 81:376–398.

Bennett, S. C. 2007b. A review of the pterosaur *Ctenochasma*: taxonomy and ontogeny. Neues Jahrbuch für Geologie und Paläontologie, Abhandlungen 245:23–31.

Bennett, S. C. 2013. New information on body size and cranial display structures of *Pterodactylus antiquus*, with a revision of the genus. Paläontologische Zeitschrift 87:269–289.

Bennett, S. C. 2017. New smallest specimen of the pterosaur *Pteranodon* and ontogenetic niches in pterosaurs. Journal of Paleontology 92:1–18.

Benson, R. B., R. J. Butler, M. T. Carrano, and P. M. O'Connor. 2012. Air-filled postcranial bones in theropod dinosaurs: physiological implications and the 'reptile'–bird transition. Biological Reviews 87:168–193.

Brower J.C., and J. Veinus. 1981. Allometry in pterosaurs. University of Kansas Paleontological Contributions, Paper 105:1–32.

Britt, B. B., F. M. Dalla Vecchia, D. J. Chure, G. F. Engelmann, M. F. Whiting, and R. D. Scheetz. 2018. *Caelestiventus hanseni* gen. et sp. nov. extends the desert-dwelling pterosaur record back 65 million years. Nature Ecology & Evolution 2:1386–1392.

Canty, A., and B. Ripley. 2021. boot: bootstrap R (S-Plus) functions. R package version 1.3-27. Available at https://cran.r-project.org/package=boot.

Chen, M., C. A. Strömberg, and G. P. Wilson. 2019. Assembly of modern mammal community structure driven by Late Cretaceous dental evolution, rise of flowering plants, and dinosaur demise. Proceedings of the National Academy of Sciences, USA 116:9931–9940.

Codorniú, L. 2007. Evidencias de cambios alométricos en las cervicales de *Pterodaustro guinazui* (Pterosauria, Pterodactyloidea). Ameghiniana 44:10.

Costa, F., V. Alifanov, F. Dalla Vecchia, and A. W. A. Kellner. 2013. On the presence of an elongated tail in an undescribed specimen of *Batrachognathus volans* (Pterosauria: Anurognathidae: Batrachognathinae). In Rio Ptero 2013-International Symposium on Pterosaurs, Short Communications 54–56.

Dalla Vecchia, F. M. 2002. Observations on the non-pterodactyloid pterosaur *Jeholopterus ningchengensis* from the Early Cretaceous of northeastern China. Natura Nascosta 24:8–27.

Dalla Vecchia, F. M. 2009. Anatomy and systematics of the pterosaur *Carniadactylus* gen. n. *rosenfeldi* (Dalla Vecchia, 1995). Rivista Italiana di Paleontologia e Stratigrafia 115:159–188.

Dalla Vecchia, F. M. 2019. *Seazzadactylus venieri* gen. et sp. nov., a new pterosaur (Diapsida: Pterosauria) from the Upper Triassic (Norian) of northeastern Italy. PeerJ 7:e7363.

Delfino, M., and M. R. Sánchez-Villagra. 2010. A survey of the rock record of reptilian ontogeny. Proceedings Seminars in Cell & Developmental Biology 21:432–440.

Dodson, P. 1975. Functional and ecological significance of relative growth in *Alligator*. Journal of Zoology 175:315–355.

Dray, S., and J. Josse. 2015. Principal component analysis with missing values: a comparative survey of methods. Plant Ecology 216:657–667.

Evans, M.R. and A.L. Thomas. 1992. The aerodynamic and mechanical effects of elongated tails in the scarlet-tufted malachite sunbird: measuring the cost of a handicap. Animal Behaviour 43:337–347.

Frey, E., M.-C. Buchy, and D. M. Martill. 2003. Middle-and bottom-decker Cretaceous pterosaurs: unique designs in active flying vertebrates. Geological Society, London, Special Publications 217:267–274.

Gao, K., Q. Li, M. Wei, H. Pak, and I. Pak. 2009. Early Cretaceous birds and pterosaurs from the Sinuiju Series, and geographic extension of the Jehol Biota into the Korean Peninsula. Journal of the Paleontological Society of Korea 25:57–61.

Goloboff, P., and J. S. Farris. 2008. TNT, a free program for phylogenetic analysis. Cladistics 24:774–786.

Gradstein, F. M., J. G. Ogg, M. D. Schmitz, and G. M. Ogg. 2012. The Geologic Time Scale 2012. Elsevier, Oxford, U.K., 1176 pp.

Henry, L., and H. Wickham. 2020. Purrr: functional programming tools. R package version 0.3.4. Available at https://cran.r-project.org/package=purrr.

Hone, D. W. E. 2020. A review of the taxonomy and palaeoecology of the Anurognathidae (Reptilia, Pterosauria). Acta Geologica Sinica 94:1676–1692.

Hone, D. W. E., M. Van Rooijen, and M. Habib. 2015. The wingtips of the pterosaurs: anatomy, aeronautical function and ecological implications. Palaeogeography, Palaeoclimatology, Palaeoecology 440:431–439.

Hone, D. W. E., J. M. Ratcliffe, D. K. Riskin, J. W. Hermanson, and R. R. Reisz. 2020. Unique near isometric ontogeny in the pterosaur

Rhamphorhynchus suggests hatchlings could fly. Lethaia 54:106–112.

Ji, Q., and C. Yuan. 2002. Discovery of two kinds of protofeathered pterosaurs in the Mesozoic Daohugou Biota in the Ningcheng region and its stratigraphic and biologic significances. Geological Review 48:221–224.

Ji, S., and Q. Ji. 1998. A new fossil pterosaur (Rhamphorhynchoidea) from Liaoning. Jiangsu Geology 22:199–206. [Chinese]

Jiang, S., X. Wang, X. Cheng, F. R. Costa, J. Huang, and A. W. A. Kellner. 2015. Short note on an anurognathid pterosaur with a long tail from the Upper Jurassic of China. Historical Biology 27:718–722.

Jiang, S., X. Wang, X. Zheng, X. Cheng, J. Zhang, and X. Wang. 2021. An early juvenile of *Kunpengopterus sinensis* (Pterosauria) from the Late Jurassic in China. Anais da Academia Brasileira de Ciências 93:e20200734.

Jolicoeur, P. 1963. The multivariate generalization of the allometry equation. Biometrics 19:497–499.

Josse, J., and F. Husson. 2012. Handling missing values in exploratory multivariate data analysis methods. Journal de la Société Française de Statistique 153:1–21.

Josse, J., and F. Husson. 2016. missMDA: a package for handling missing values in multivariate data analysis. Journal of Statistical Software 70:1–31.

Jouve, S. 2004. Description of the skull of *Ctenochasma* (Pterosauria) from the latest Jurassic of eastern France, with a taxonomic revision of European Tithonian Pterodactyloidea. Journal of Vertebrate Paleontology 24:542–554.

Kaup, S. S. 1834. Versuch einer Eintheilung der Saugethiere in 6 Stämme und der Amphibien in 6 Ordnung. Isis von Oken 1834:311–324.

Kellner, A. W. A. 2003. Pterosaur phylogeny and comments on the evolutionary history of the group. Geological Society, London, Special Publications 217:105–137.

Kellner, A. W. A., X. Wang, H. Tischlinger, D. de A. Campos, D. W. E. Hone, and X. Meng. 2010. The soft tissue of *Jeholopterus* (Pterosauria, Anurognathidae, Batrachognathidae) and the structure of the pterosaur wing membrane. Proceedings of the Royal Society B 277:321–329.

Kiers, H. 1997. Weighted least squares fitting using ordinary least squares algorithms. Psychometrika 62:251–266.

Klingenberg, C. P. 1996. Multivariate allometry; pp. 23–49 in L. F. Marcus, M. Corti, A. Loy, G. J. P. Naylor and D. E. Slice (eds.), Advances in Morphometrics. Plenum Press, New York.

Kuhn, O. 1937. Die fossilen Reptilien. Gebrüder Borntraeger, Berlin, 121 pp.

Longrich, N.R., D.M. Martill, and B. Andres. 2018. Late Maastrichtian pterosaurs from North Africa and mass extinction of Pterosauria at the Cretaceous-Paleogene boundary. PLoS Biology 16:e2001663.

Lü, J., and D. W. E. Hone. 2012. A new Chinese anurognathid pterosaur and the evolution of pterosaurian tail lengths. Acta Geologica Sinica 86:1317–1325.

Lü, J., and Q. Ji. 2006. Preliminary results of a phylogenetic analysis of the pterosaurs from western Liaoning and surrounding areas. Journal of the Paleontological Society of Korea 22:239–261.

Lü, J., D. M. Unwin, X. Jin, Y. Liu, and Q. Ji. 2010. Evidence for modular evolution in a long-tailed pterosaur with a pterodactyloid skull. Proceedings of the Royal Society B 277:383–389.

Lü, J., Q. Meng, B. Wang, D. Liu, C. Shen, and Y. Zhang. 2018. Short note on a new anurognathid pterosaur with evidence of perching behaviour from Jianchang of Liaoning Province, China. Geological Society, London, Special Publications 455:95–104.

Lü, J., D. M. Unwin, D. C. Deeming, X. Jin, Y. Liu, and Q. Ji. 2011. An egg-adult association, gender, and reproduction in pterosaurs. Science 331:321–324.

Mayer, F., and O. v. Helversen. 2001. Cryptic diversity in European bats. Proceedings of the Royal Society B 268:1825–1832.

Naish, D., M. P. Witton, and E. Martin-Silverstone. 2021. Powered flight in hatchling pterosaurs: evidence from wing form and bone strength. Scientific Reports 11:1–5.

Ősi, A. 2011. Feeding-related characters in basal pterosaurs: implications for jaw mechanism, dental function and diet. Lethaia 44:136–152.

Padian, K., and K. I. Warheit. 1989. Morphometrics of the pterosaur wing: one sharp division, few trends. Journal of Vertebrate Paleontology 9:35A.

Plotnick, R. E. 1989. Application of bootstrap methods to reduced major axis line fitting. Systematic Biology 38:144–153.

Schepelmann, K. 1990. Erythropoietic bone marrow in the pigeon: development of its distribution and volume during growth and pneumatization of bones. Journal of Morphology 203:21–34.

Shaw, J. B. 2011. Evolution and development of wing form, body size and flight in large-and small-bodied fruit bats (*Artibeus jamaicensis* and *Carollia perspiciillata*). Ph.D. dissertation, University of Northern Colorado, Greeley, Colorado, 253 pp.

Tomkins, J. L., N. R. LeBas, M. P. Witton, D. M. Martill, and S. Humphries. 2010. Positive allometry and the prehistory of sexual selection. American Naturalist 176:141–148.

Unwin, D. M. 2003a. *Eudimorphodon* and the early history of pterosaurs. Rivista del Museo Civico di Scienze Naturali "Enrico Caffi" 22:39–46.

Unwin, D. M., 2003b, On the phylogeny and evolutionary history of pterosaurs. Geological Society, London, Special Publications 217:139–190.

Unwin, D. M. 2005. The pterosaurs from deep time. Pi Press, New York, 347 pp.

Unwin, D. M., and N. N. Bakhurina. 2000. Pterosaurs from Russia, Middle Asia and Mongolia; pp. 420–433 in M. J. Benton, M.A. Shishkin, D. M. Unwin, and E. N. Kurochkin (eds.), The age of dinosaurs in Russia and Mongolia. Cambridge University Press, Cambridge.

Unwin, D. M., and D. C. Deeming. 2019. Prenatal development in pterosaurs and its implications for their postnatal locomotory ability. Proceedings of the Royal Society B 286:20190409.

Unwin, D. M., J. Lü, and N. N. Bakhurina. 2000. On the systematic and stratigraphic significance of pterosaurs from the Lower Cretaceous Yixian Formation (Jehol Group) of Liaoning, China. Fossil Record 3:181–206.

Vidovic, S. U., and D. M. Martill. 2014. *Pterodactylus scolopaciceps* Meyer, 1860 (Pterosauria, Pterodactyloidea) from the Upper Jurassic of Bavaria, Germany: the problem of cryptic pterosaur taxa in early ontogeny. PLoS ONE 9:e110646.

Vidovic, S. U., and D. M. Martill. 2018. The taxonomy and phylogeny of *Diopecephalus kochi* (Wagner, 1837) and '*Germanodactylus rhamphastinus*' (Wagner, 1851). Geological Society, London, Special Publications 455:125–147.

Viscardi, P., G. Dyke, M. Wilkinson, and J. Rayner. 1999. Missing data and the phylogeny of the Pterosauria. Journal of Vertebrate Paleontology 19:83A.

Wang, X., A. W. A. Kellner, Z. Zhou, and D. A. Campos. 2005. Pterosaur diversity and faunal turnover in Cretaceous terrestrial ecosystems in China. Nature 437:875–879.

Wang, X., A. W. A. Kellner, Z. Zhou, and D. A. Campos. 2008. Discovery of a rare arboreal forest-dwelling flying reptile (Pterosauria, Pterodactyloidea) from China. Proceedings of the National Academy of Sciences, USA 105:1983–1987.

Wang, X., Z. Zhou, F. Zhang, and X. Xu. 2002. A nearly completely articulated rhamphorhynchoid pterosaur with exceptionally well-preserved wing membranes and "hairs" from Inner Mongolia, northeast China. Chinese Science Bulletin 47:226–230.

Wang, X., S. Jiang, J. Zhang, X. Cheng, X. Yu, Y. Li, G. Wei, and X. Wang. 2017. New evidence from China for the nature of the pterosaur evolutionary transition. Scientific Reports 7:42763.

Warton, D. I., R. A. Duursma, D. S. Falster, and S. Taskinen. 2012. smatr 3–an R package for estimation and inference about allometric lines. Methods in Ecology and Evolution 3:257–259. R package version 3.4-8. Available at https://cran.r-project.org/package=smatr.

Wedel, M. J. 2003. The evolution of vertebral pneumaticity in sauropod dinosaurs. Journal of Vertebrate Paleontology 23:344–357.

Wei, X., R.V. Pêgas, C. Shen, Y. Guo, W. Ma, D. Sun and X. Zhou. 2021. *Sinomacrops bondei*, a new anurognathid pterosaur from the Jurassic of China and comments on the group. PeerJ 9:e11161.

Wellnhofer, P. 1970. Die Pterodactyloidea (Pterosauria) der Oberjura-Plattenkalke Süddeutschlands. Bayerische Akademie der Wissenschaften, Mathematisch-Wissenschaftlichen Klasse, Abhandlungen 141:1–133.

Wellnhofer, P. 1975. Die Rhamphorhynchoidea (Pterosauria) der Oberjura-Plattenkalke Süddeutschlands. Palaeontographica A 148:1–33, 148:132–186, 149:1–30.

Werner, E. E., and J. F. Gilliam. 1984. The ontogenetic niche and species interactions in size-structured populations. Annual review of Ecology and Systematics 15:393–425.

Wickham, H., R. Francois, L. Henry, and K. Müller. 2015. dplyr: a grammar of data manipulation. R package version 0.8.1. Available at https://cran.r-project.org/package=dplyr.

Witton, M. P. 2008. A new approach to determining pterosaur body mass and its implications for pterosaur flight. Zitteliana B 28:143–158.

Witton, M. P., and M. B. Habib. 2010. On the size and flight diversity of giant pterosaurs, the use of birds as pterosaur analogues and comments on pterosaur flightlessness. PLoS ONE 5:e13982.

Xu, X., Z. Zhou, C. Sullivan, Y. Wang, and D. Ren. 2016. An updated review of the Middle-Late Jurassic Yanliao Biota: chronology, taphonomy, paleontology and paleoecology. Acta Geologica Sinica 90:2229–2243.

Yang, Z., B. Jiang, M. E. McNamara, S. L. Kearns, M. Pittman, T. G. Kaye, P. J. Orr, X. Xu, and M. J. Benton. 2019. Pterosaur integumentary structures with complex feather-like branching. Nature Ecology & Evolution 3:24–30.

Submitted December 21, 2020; revisions received October 15, 2021; accepted January 3, 2022.
Handling Editor: Elizabeth Martin-Silverstone.